

FLOW FIELD EVOLUTION OF A DECAYING SUNSPOT

NA DENG AND DEBI PRASAD CHOUDHARY

California State University Northridge, Physics and Astronomy Department, 18111 Nordhoff St., Northridge, CA 91330;
 na.deng@csun.edu, debiprasad.choudhary@csun.edu

ALEXANDRA TRITSCHLER

National Solar Observatory/Sacramento Peak*, P.O. Box 62, Sunspot, NM 88349, U.S.A.; ali@nso.edu

CARSTEN DENKER¹

Astrophysikalisches Institut Potsdam, An der Sternwarte 16, D-14482 Potsdam, Germany; cdenker@aip.de

CHANG LIU AND HAIMIN WANG

New Jersey Institute of Technology, Physics Department, Center for Solar-Terrestrial Research, 323 Martin Luther King Blvd, Newark, NJ 07102

Big Bear Solar Observatory, 40386 North Shore Lane, Big Bear City, CA 92314, U.S.A.; cliu@bbso.njit.edu, haimin@flare.njit.edu

Draft version February 2, 2008

ABSTRACT

We study the evolution of the flows and horizontal proper motions in and around a decaying follower sunspot based on time sequences of two-dimensional spectroscopic observations in the visible and white light imaging data obtained over six days from June 7 to 12, 2005. During this time period the sunspot decayed gradually to a pore. The spectroscopic observations were obtained with the Fabry-Pérot based Visible-Light Imaging Magnetograph (VIM) in conjunction with the high-order adaptive optics (AO) system operated at the 65 cm vacuum reflector of the Big Bear Solar Observatory (BBSO). We apply local correlation tracking (LCT) to the speckle reconstructed time sequences of white-light images around 600 nm to infer horizontal proper motions while the Doppler shifts of the scanned Fe I line at 630.15 nm are used to calculate line-of-sight (LOS) velocities with sub-arcsecond resolution. We find that the dividing line between radial inward and outward proper motions in the inner and outer penumbra, respectively, survives the decay phase. In particular the moat flow is still detectable after the penumbra disappeared. Based on our observations three major processes removed flux from the sunspot: (a) fragmentation of the umbra, (b) flux cancelation of moving magnetic features (MMFs; of the same polarity as the sunspot) that encounter the leading opposite polarity network and plage areas, and (c) flux transport by MMFs (of the same polarity as the sunspot) to the surrounding network and plage regions that have the same polarity as the sunspot.

Subject headings: Sun: activity — Sun: photosphere — sunspots — instrumentation: high angular resolution — instrumentation: spectrographs — techniques: spectroscopic

1. INTRODUCTION

The evolution of active regions has been extensively studied for decades (e.g. Solanki 2003, and references therein). While much progress has been achieved in understanding of how flux is transported from deep in the convection zone to emerge at the solar surface in form of sunspots, a comprehensive picture of the regularities underlying the decay process (e.g. Martínez Pillet 2002) is still missing. Typically, a statistical approach is followed to characterize the decay phase by changes in umbral and penumbral brightness, magnetic flux, or area in an attempt to find either a common (mean) decay law (e.g. Moreno-Insertis & Vazquez 1988; Petrovay et al. 1999) or by studying the distribution of the decay rates (e.g. Martínez Pillet et al. 1993). However, this strategy does only evaluate the behavior of groups rather than of in-

dividual sunspots and does not give detailed insight into the individual processes that might contribute to or trigger the decay process.

The decay phase of a sunspot can be initiated at any time (McIntosh 1981) and proceeds differently for individual sunspots. Chapman et al. (2003) analyzed the decay phase of many sunspots and found a strong correlation between the sunspot photometric decay rate, the total sunspot area and the umbral to total area ratio. By carefully measuring the magnetic flux, Zwaan (1992) detected no significant increase in the total magnetic flux of the sunspot after the penumbra is formed. Furthermore, Leka & Skumanich (1998) observed that the umbral flux does not decrease during the formation of a penumbra. These findings suggest that the formation and decay of penumbrae is not immediately related to changes in the sunspot magnetic flux, but rather a phenomenon related to a change in the local flow field in and around the flux concentration. Differences between the flow field around the sunspot and that around the umbral fragments and pores thus might allow to determine critical conditions

*Operated by the Association of Universities for Research in Astronomy, Inc. (AURA), for the National Science Foundation

¹ New Jersey Institute of Technology, Physics Department, Center for Solar-Terrestrial Research, 323 Martin Luther King Blvd, Newark, NJ 07102, U.S.A.

necessary for both penumbral formation and decay.

The most prominent flow spectroscopically measured in a sunspot is the Evershed flow (Evershed 1909), which reveals itself in form of shifts and asymmetries of solar spectral lines and which is interpreted as an outward mass flow in the photospheric layers of penumbrae. The Evershed effect is intrinsically coupled to the presence of a penumbra and ceases at the immediate outer penumbral border. Leka & Skumanich (1998) and Yang et al. (2003) detected an Evershed flow as soon as the magnetic field lines reached a critical inclination and organized filamentary structures became visible. The Evershed flow itself varies quasi-periodically in time (Shine et al. 1994; Rimmele 1994; Rouppe van der Voort 2003; Cabrera Solana et al. 2006), which is predominantly caused by velocity patches that propagate along penumbral filaments from the middle penumbra to the outer penumbra, the so-called Evershed clouds (ECs) which were first observed and named by Shine et al. (1994). In their most recent study, Cabrera Solana et al. (2007) identify two classes of ECs, those that vanish directly at the outer penumbral boundary and those that cross the visible border and enter the moat flow. Once detached from the penumbra, these ECs survive ~ 14 min before they disappear in close proximity to the spot ($\sim 2''$). The outward migration of the ECs could give a natural explanation for the existence of a dividing line within the penumbra separating features that move inwards in the inner penumbra and outwards in the outer penumbra. This dividing line appears typically in horizontal proper motion maps derived from either local correlation tracking (e.g. November 1986; November et al. 1986) or pattern recognition (e.g. Sobotka et al. 1999; Bovelet & Wiehr 2003). Molowny-Horas (1994) was the first to identify such a ring-like dividing area, featuring near-zero horizontal speed and constant velocity divergence.

The sunspot moat is a zone that surrounds most mature sunspots and some large sunspot pores. The moat region is characterized by a radially directed outward mass flow. Although the moat is free of stationary magnetic fields, time sequences of magnetograms show moving magnetic features (MMFs), i.e., small-scale magnetic flux concentrations of mixed polarity, that move along with the moat flow in radial direction away from the sunspot (Sheeley 1969; Harvey & Harvey 1973; Brickhouse & Labonte 1988; Yurchyshyn & Wang 2001; Hagenaar & Shine 2005; Kubo et al. 2007; Choudhary & Balasubramaniam 2007). There is increasing evidence that the Evershed flow, the moat flow, and MMFs are closely related to each other (e.g. Sainz Dalda & Martínez Pillet 2005; Ravindra 2006; Cabrera Solana et al. 2006). In a case study Vargas Domínguez et al. (2007) find that for a complex active region the existence of the moat flow is coupled to the presence of penumbral filaments. Hence, the moat should neither be found around individual pores or umbral fragments after the penumbra disappeared. However, observational results differ considerably depending on what type of sunspot and pores have been observed and what techniques have been used (see e.g. Wang & Zirin 1992; Denker 1998; Yang et al. 2003).

In this paper, we study the evolution of line-of-sight

(LOS) flows and horizontal proper motions in and around a decaying sunspot. Our investigation is based on sequences of high-spatial resolution observations obtained over six days with new post-focus instrumentation at the Big Bear Solar Observatory (BBSO) (Denker et al. 2005; Denker & Tritschler 2005; Denker et al. 2007b). Both the LOS velocities measured from two-dimensional spectroscopic observations and horizontal proper motions derived with local correlation tracking (LCT) technique based on speckle reconstructed images are analyzed. In §2 we overview the two-dimensional spectroscopic and speckle imaging observations. The data reduction is described in §3 and the results are presented in §4. We discuss the results and offer our conclusions in §5.

2. OBSERVATIONS

The observations were performed with BBSO's 65 cm vacuum reflector in conjunction with the high-order adaptive optics (AO) system (Rimmele et al. 2004; Denker et al. 2007b). We observed the isolated follower spot of active region NOAA 10773 during its disk passage on five days in summer 2005: June 7 ($\mu \approx 0.96$), June 8 ($\mu \approx 0.95$), June 10 ($\mu \approx 0.77$), June 11 ($\mu \approx 0.61$), and June 12 ($\mu \approx 0.43$). Two-dimensional spectroscopic scans of the photospheric spectral line Fe I 630.15 nm were obtained with the Visible-light Imaging Magnetograph (VIM) system, in which a single Fabry-Pérot etalon is the core element (Denker & Tritschler 2005). VIM has a bandpass of 8 pm. A 0.3 nm wide prefilter centered on the Fe I 630.15 nm line was used before the Fabry-Pérot etalon. The Fe I line was sampled at 101 equidistant wavelength points with a step size of 1.2 pm corresponding to a scanned wavelength interval of 0.12 nm. The exposure time at each wavelength point was 80 ms. The cadence of each scan was about 18 s. A total of 100 scans can be obtained in 30 min, which was the typical time range of an observing run. The spectroscopic data have a field-of-view (FOV) of about $74'' \times 74''$. The $1k \times 1k$ CCD camera was operated in a 2×2 pixel binning mode. Thus, the image scale was about $0.14'' \text{ pixel}^{-1}$. The spatial resolution achieved by the spectroscopic scans is estimated at about $0.5''$ with power spectrum analysis.

The spectroscopic observations are supported by quasi-synchronous bursts of short-exposure (10 ms) white-light images at 600 ± 5 nm recorded with a fast CCD camera system for image restoration. Every 30 s, a total of 200 frames was captured at 15 frames s^{-1} , from which the best 100 frames were automatically selected and combined to create one restored image using a speckle masking algorithm (Denker et al. 2005). The cadence of the reconstructed white-light images is thus 30 s. A total of 60 reconstructed images were obtained in a 30 min observing run. The FOV is about $70'' \times 70''$ and the image scale is about $0''.07 \text{ pixel}^{-1}$. The spatial resolution of the reconstructed images is diffraction limited ($\approx 0.25''$) by the 65 cm reflector of the BBSO if we use $1.22\lambda/D$ as the measure of the diffraction limit. Each observing run typically lasted 30 min. Further details of the observations are given by Denker et al. (2007b,a), who provide a thorough description of the high-resolution observations and a performance evaluation of the AO system.

Figure 1 shows the sunspot observed on June 7 in a speckle reconstructed white-light image (panel a) and the

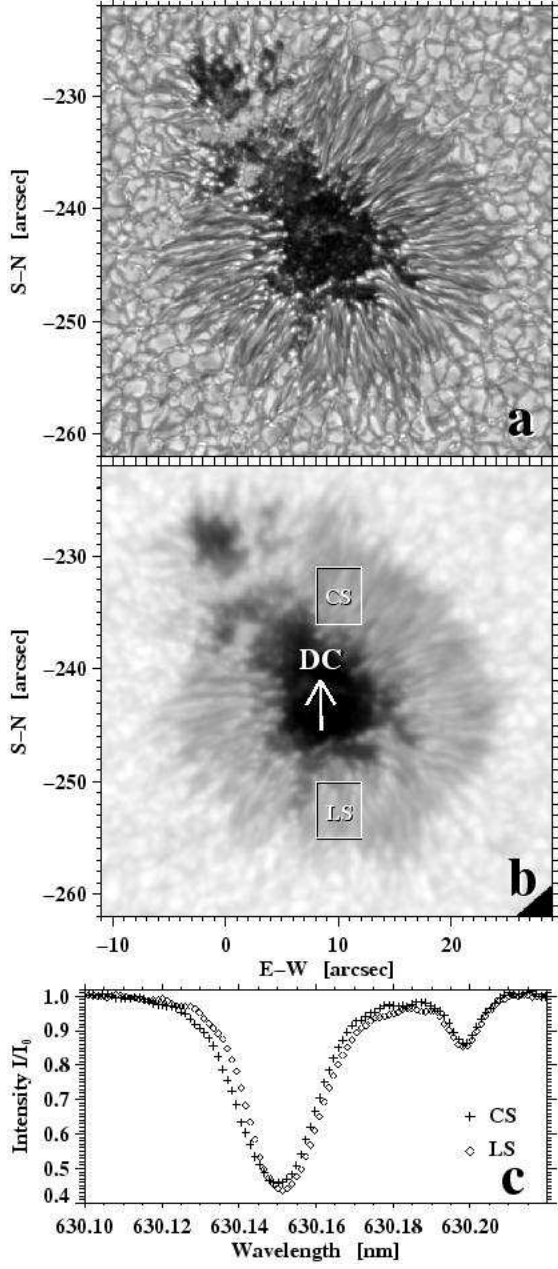


FIG. 1.— *a*: Speckle reconstructed white-light image of the follower sunspot in active region NOAA 10773 on 2005 June 7. *b*: Corresponding continuum intensity image observed with the two-dimensional spectrometer. The white arrow points towards the disk center (DC). *c*: Sample line profiles of the two-dimensional spectroscopy averaged over small areas in the center-side (CS) and limb-side (LS) penumbra, which are indicated by white boxes in *b*.

corresponding continuum intensity image obtained with VIM (panel *b*). Panel *c* shows two sample line profiles averaged over a small area of limb-side (LS) and center-side (CS) penumbra, which are indicated in panel *b* by white boxes. The two profiles are shifted w.r.t. each other indicating the Evershed flow. The reconstructed image clearly shows the sunspot fine structure, such as numerous umbral dots, the penumbral dark cores, and the twist and writhe of the penumbral filaments. We also note that the penumbral grains are brighter on the limb-side of the penumbra.

NOAA 10773 was also monitored by BBSO's 25 cm re-

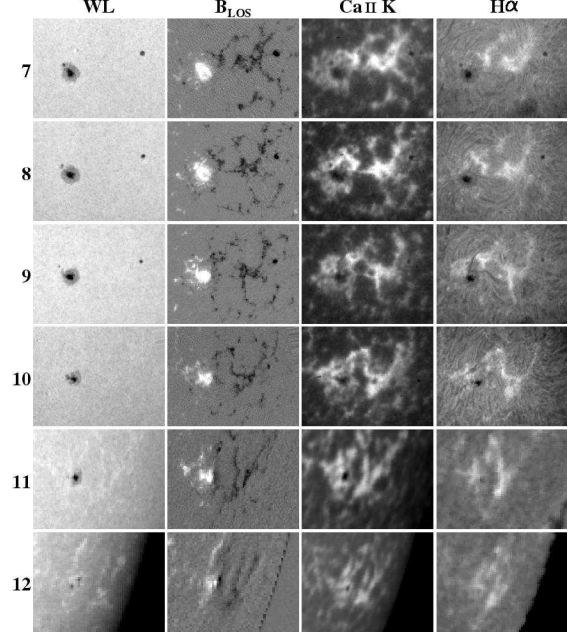


FIG. 2.— Evolution of active region NOAA 10773 from 2005 June 7 to June 12. The columns (from left to right) represent white-light (WL) images, LOS magnetic field B_{LOS} , and Ca II K and H α filtergrams.

fractor. These context observations include vector magnetograms as well as H α and Ca II K filtergrams. Figure 2 shows the whole active region and its evolution over six consecutive days based on white-light information, LOS magnetograms, and Ca II K and H α filtergrams. BBSO's LOS magnetograms are produced by dividing the difference between the right- and left-hand circularly polarized Stokes components by their sum under weak field approximation. They suffer from the problem of Zeeman saturation when the field is stronger than typically 3000 G (Wang et al. 1998; Spirock 2005). We employ data from other observatories on some days because no synoptic BBSO data were available. For example, the white-light and magnetogram data on June 9, 11, and 12 are from the Michelson Doppler Imager (MDI, Scherrer et al. 1995) on board the Solar and Heliospheric Observatory. The Ca II K and H α filtergrams on June 11 and 12 are from the Mauna Loa Solar Observatory operated by the High Altitude Observatory. The active region was in the southern hemisphere (S15°). The target was a relatively stable, round follower sunspot with positive magnetic polarity located on the left side in the panels of Figure 2. The leading spot on the right side was otherwise smaller in size. This configuration is an exception, since the leading spot is typically more stable and larger in size. The bright areas in Ca II K and H α filtergrams trace the plage regions that are spatially correlated with magnetic fields of the supergranular network.

3. DATA REDUCTION

We apply standard procedures such as dark subtraction and gain table correction to the spectroscopic observations and white-light images. The speckle reconstructions and the scans are carefully co-aligned with each other. The white-light images were also co-aligned with the corresponding MDI intensity images in order to acquire accurate locations and orientations of the sunspot

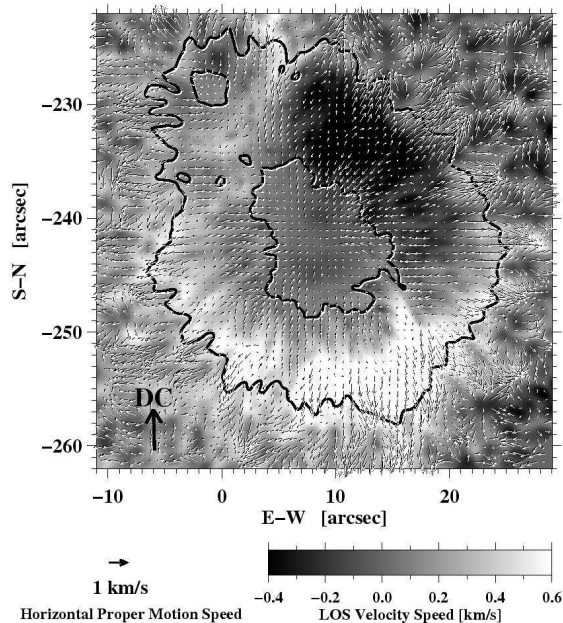


FIG. 3.— Combination of LOS dopplergram and LCT horizontal proper motions of the observed sunspot (NOAA 10773) on 2005 June 7. Arrows show a 30-minute average of LCT proper motion maps derived from speckle-restored images. The gray-scale background image represents the LOS velocity, which is the corresponding 30-minute average of the dopplergrams. Redshifts are positive and correspond to bright areas. The black contours outline the umbral and penumbral boundaries.

on different days. In order to remove the 5-minute oscillation and residual seeing distortions a subsonic filter with a phase velocity threshold of 4 km s^{-1} was applied to the time-series of white-light speckle and spectroscopic data.

The LOS velocity is determined by a Fourier phase method (see Schmidt et al. 1999), which uses the entire Fe I 630.15 nm line profile and is very insensitive to noise. The telluric blend at 630.2 nm is not included in the calculation. The determined shifts are converted to velocities by using the Doppler formula. As a frame of reference we use the average velocity of a small area in the darkest part of the umbra or pore. The final calibrated dopplergrams follow the convention that redshifts are positive and blueshifts are negative. Thus, bright areas in the dopplergrams move away from the observer, while dark areas move towards the observer. The Fe I 630.15 nm has a non-negligible Landé factor and is thus susceptible to the presence of magnetic fields. The influence of the magnetic field on the line shape, however, is symmetric with respect to the line core and should not significantly influence the velocity determination.

The ANA implementation (<http://ana.lmsal.com/ana/>) of the LCT algorithm (November 1986; November et al. 1986) was applied to each of the individual 30-minute observing sequences of speckle reconstructions. A Gaussian shape apodization window with a FWHM of $1.4''$ (corresponding to the mean size of the granulation) was used in the LCT technique. Since each sequence consists of 60 reconstructions, this resulted in 59 individual LCT proper motion maps. The individual proper motion maps are averaged to achieve a significant reduction of seeing induced random noise. Furthermore, we use inverse

cork maps to visualize sources of divergence in a LCT proper motion map (see e.g. Molowny-Horas 1994; Denker 1998). A total of 22,500 corks (artificial tracer particles) were distributed evenly across the average LCT proper motion map. Their movement is traced for 10 h backwards in time. The corks concentrate at positions where the proper motion shows strong and persistent divergence. The resulting cork map traces the location of the dividing line between inward and outward horizontal proper motions in the sunspot penumbra. It should be mentioned that all the quantities and figures presented in this paper, unless otherwise noted, have been corrected for perspective foreshortening.

To demonstrate the outcome of the described methodology Figure 3 displays the average LCT proper motion map superposed on the LOS dopplergram averaged over the same time period for 2005 June 7. It clearly shows the Evershed effect in the background LOS dopplergram, and visualizes the inward motion in the inner penumbra and outward motion in the outer penumbra as indicated by the arrows showing the horizontal proper motion. The outward proper motion exceeds the outer penumbral boundary by $3''$ to $5''$ while the LOS Evershed flow ceases more or less abruptly at the visible boundary of the outer penumbra. Moreover, we detect diverging and converging trends in the radial outward proper motions outside the sunspot.

4. RESULTS

Figure 4 illustrates the result of the cork analysis based on the reconstructed white-light images for all observing days. The white contours mark the umbral and penumbral boundaries as derived from intensity thresholds set to 60 % and 90 % of the quiet Sun intensity, respectively. The yellow dots indicate the corks that are swept to regions where the horizontal proper motion is not divergence free. Figure 4 clearly reveals the dividing lines, which separate the inward and outward proper motions in the penumbra. The dividing lines always reside inside the penumbra. They tend to be more symmetric when the sunspot penumbra itself has a more symmetric shape (see panel *b* in Figure 4). They lose symmetry when the sunspot penumbra becomes less symmetric (see the other panels in Figure 4). Interestingly, even after the penumbra completely disappeared, there is still a distinct dividing line around the remaining pore, although, incomplete and disrupted at some locations (see panel *f* in Figure 4).

The average LCT proper motion vectors (see Figure 3) are decomposed into two components, i.e., magnitude $|v_{\text{LCT}}|$ and azimuthal direction ϕ_{LCT} . They are displayed for each pixel in Figure 5. From June 7 to June 11, when the sunspot has a penumbra, the ϕ_{LCT} component shows a radial inward motion in the inner sunspot (including the umbra and the inner part of penumbra) and a radial outward motion in the outer sunspot. The outward motion extends beyond the visible boundary of the outer penumbra for up to $5''$. In other words, a $5''$ wide annular zone showing a radial outward proper motion (collar flow) surrounds the penumbra (or the sunspot). The $|v_{\text{LCT}}|$ component shows that there are two ring-like proper motion structures with large $|v_{\text{LCT}}|$ values. One is surrounding the penumbra-umbra interface corresponding to the inward motion of penumbral grains, which has relatively small magnitude (with average speeds of

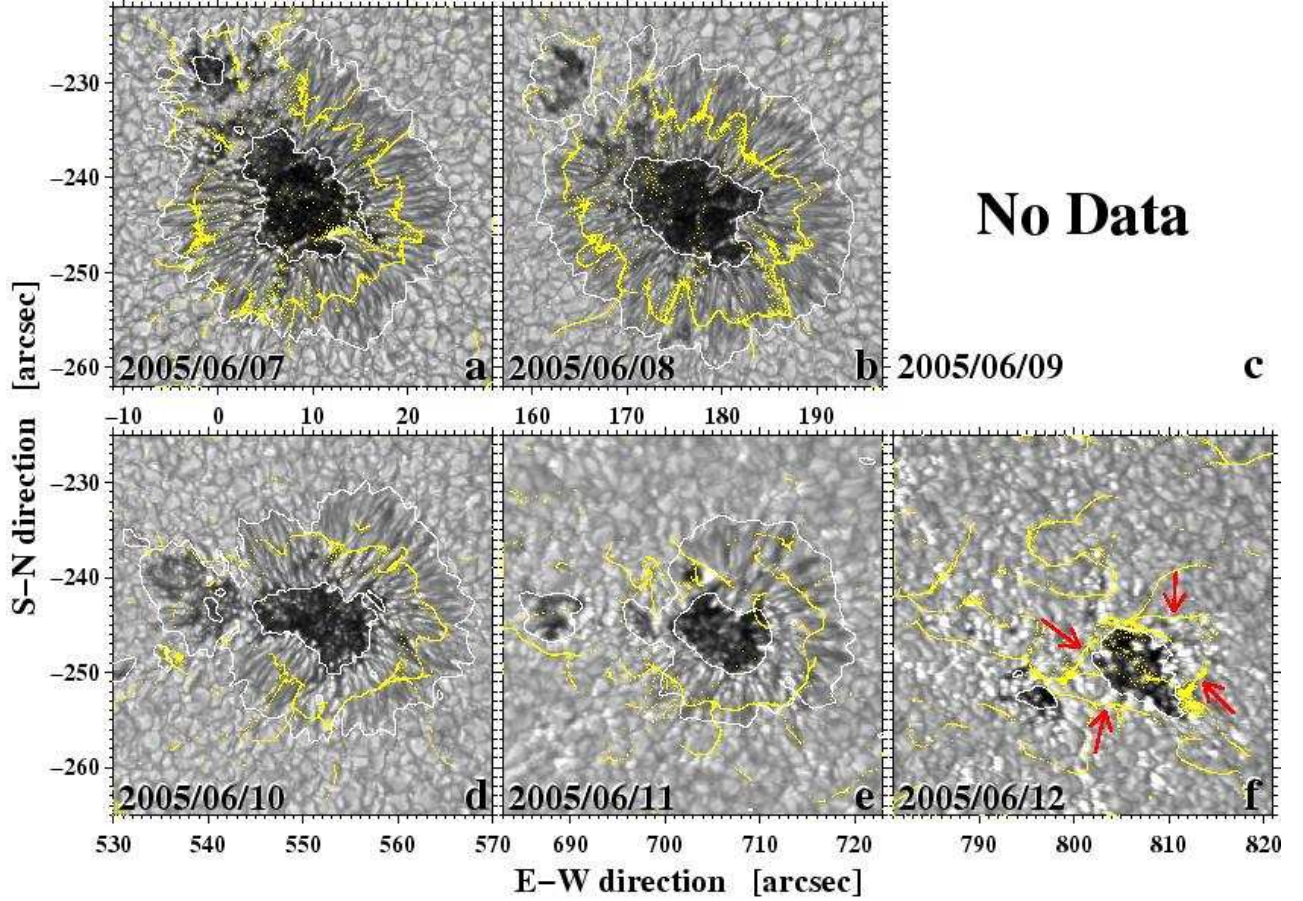


FIG. 4.— Sunspot evolution over six days during its decaying phase. White contour lines mark the umbral and penumbral boundaries determined from 60 % and 90 % of the quiet Sun intensity, respectively. The yellow corks trace the dividing lines between the inward and the outward proper motions in the penumbra and around the residual pore. The red arrows in panel *f* point to the broken and distorted dividing line around the pore.

about 0.4 km s^{-1} and a maximum speed reaching up to 0.8 km s^{-1}). Its width is about $3''$ ($\sim 2200 \text{ km}$). The other is surrounding the outer penumbra and harbors the high speed portion of the outward motion of penumbral structures and the immediate part of the moat zone. There the $|v_{\text{LCT}}|$ component exhibits a larger magnitude with an average speed of about 0.8 km s^{-1} and a maximum speed reaching up to 1.4 km s^{-1} . Its width is about $5''$ ($\sim 3700 \text{ km}$). November et al. (1987) were the first to detect a radial, large speed collar flow of granules from the penumbra into the immediate surroundings from the flow field around sunspots and named it “annulus”. The ring-like motion patterns lose their symmetry when the sunspot decays. Both inner and outer ring seem to be shifted towards the limb-side for about $2''$ or 1500 km . As can be seen in Figure 5, the rings at the center-side occur at the penumbra-granulation or penumbra-umbra boundary, while the rings at the limb-side occur outside corresponding borders.

Concentrating on the residual pore on June 12, we see from the ϕ_{LCT} component that there is still a confined region ($\sim 2''$ to $3''$) around the pore where we detect a horizontal proper motion towards the pore, which is also indicated by the dividing line seen in Figure 4. Beyond the dividing line ϕ_{LCT} indicates a motion that is directed away from the pore. The $|v_{\text{LCT}}|$ component shows that both the inward and outward motion in and around the

pore are not as strong as those in and around the sunspot.

The LOS dopplergrams are displayed in Figure 6 for each day corresponding to the arrangement in Figure 4. The dopplergrams illustrate not only the dominant Evershed effect, but also the fine structure in the LOS velocity of the whole sunspot. This includes an indication of upflows (dark blueshifts) in umbral dots, the presence of penumbral flow channels, and upflows in penumbral grains, which are more prominent on the limb-side of the penumbra with a bright redshifted background. Furthermore, the dopplergrams corroborate the results derived from LCT proper motion maps and the cork analysis. In particular, the LOS flow field around the pore on June 12 strongly suggests that the moat flow is still present: on the limb side and center side of the pore we observe a large patch of redshifts and blueshifts, respectively. At the large viewing angle ($\mu = 0.43$), where also higher layers of the solar atmosphere are probed, the moat flow component adds significantly to the convective flow pattern in such a way that it increases the LOS component of the granular upflows on the center side but overcompensates the LOS component of the granular upflows limbwards of the pore. It is noticed that the dopplergrams for June 11 and 12 show much stronger LOS velocities far from the spot or pore than observations nearer disk center (e.g., June 7). The reason for that could be the convection of the supergranulation that contributes more

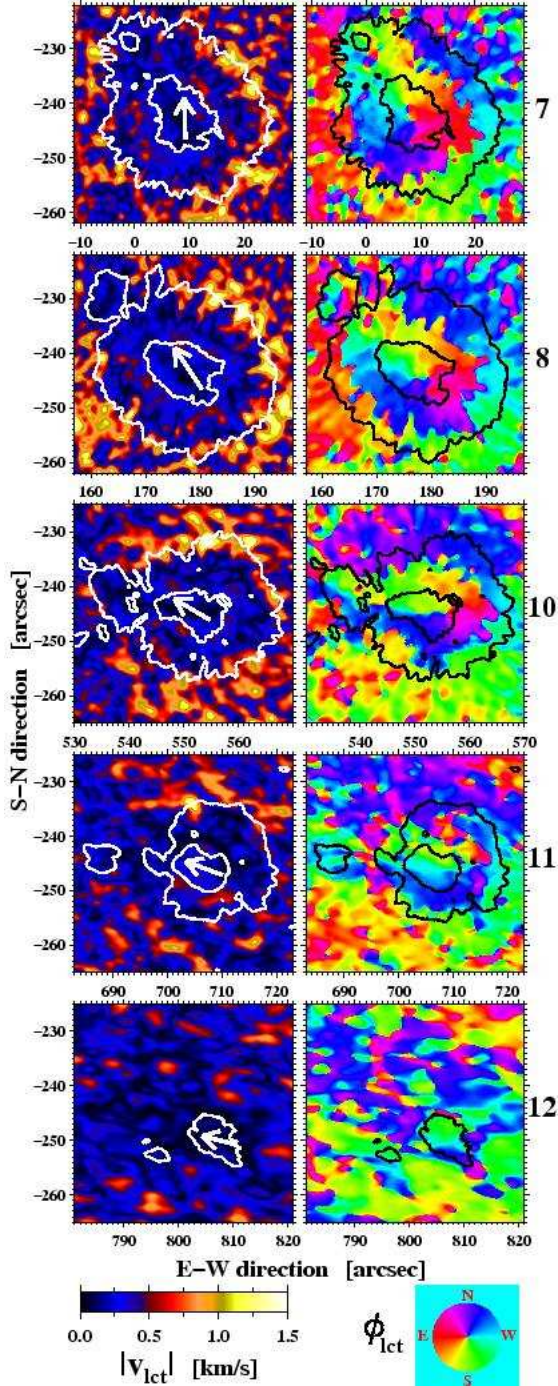


FIG. 5.— Decomposition of the 30 min average horizontal proper motions derived from LCT into speed ($|v_{\text{LCT}}|$, left) and azimuth maps (ϕ_{LCT} , right). The white or black contours outline the umbral and penumbral boundaries of the sunspot. The white arrows in the umbrae point towards the direction of disk center. The magnitude of the speed is indicated by the color scale and the azimuth angle is indicated by the color-coded disk.

to the LOS velocity towards the limb.

From Figures 2 and 4, and by watching long-term intensity and magnetogram movies from MDI, our visual impression is that magnetic flux was removed from the sunspot by the following processes: fragmentation of the spot in the north-eastern part and by MMFs. To the west, the flux transported by those MMFs that have the same polarity as the spot was promptly canceled by the

leading negative flux when the MMFs reached the outer edge of the moat region. To the east where the network and plage showed much less opposite polarity flux, substantial amount of flux was transported by MMFs of the same polarity as the sunspot into the surrounding plage region of the same polarity. Fragmentation, flux cancellation, and transport of flux to the network and plage region were likely responsible for the decay of the sunspot. On June 12, the penumbra completely disappeared and only a pair of pores remained. In addition, the sunspot had rotated counterclockwise by about 45° during the five days from June 7 to June 11.

We also noticed that the relative brightness of both penumbra and umbra increased when the sunspot moved from disk center to the limb. Moreover, this brightness increase is faster in the umbra than in the penumbra. The decay of the sunspot could be responsible for the overall increase of the sunspot brightness. Another possibility is that the sunspot is relatively brighter from the lower to the upper photosphere, which suggests that the temperature along magnetic flux tube increases faster than that in weak or non-magnetic plasmas. This behavior of the thermal stratification agrees well with the cool umbral model of Collados et al. (1994).

To illustrate the decay process of the sunspot more quantitatively we determined the change of the total sunspot area and the magnetic flux with time. The result is shown in Fig. 7. The light and dark gray vertical bars represent the penumbral and umbral areas, respectively. Their sum corresponds to the total area of the sunspot. The areas were calculated using the high-resolution data based on the enclosed areas shown by contours in Figure 4. The total-to-umbral area ratio ($r_A = A_{\text{tot}}/A_U$) and the percentage of the umbral to total sunspot area for each day were also calculated and annotated accordingly on the top and at the bottom of each bar in Figure 7, respectively. The published results of r_A range from 4.0 to 6.3, but are mostly distributed between 5.0 and 6.0 (for a summary see Solanki 2003). The result from this study shows that r_A ranges from 5.19 to 6.31, which is in agreement with previous measurements. The percentage of the umbral to total sunspot area increased from 15.85% to 18.98% from June 8 to June 11, which indicates that the sunspot penumbra decays faster than the umbra. The plus signs in Figure 7 show the evolution of the magnetic flux in the sunspot ($F = \int B \cdot dS$) calculated from MDI magnetograms. The projection effect of the area S has been corrected and the magnetic fields B were partially corrected assuming that the field lines are horizontal in the penumbra and vertical in the umbra. From June 9 to 12, the sunspot flux decayed with an almost constant decay rate of $3.2 \times 10^{15} \text{ Mx s}^{-1}$.

5. DISCUSSION AND CONCLUSION

A photometric and spectroscopic high-resolution study has been presented showing the flow fields in a decaying, isolated, quasi-round sunspot covering five days in June 2005. Based on horizontal proper motions and LOS flow fields determined from a LCT analysis and spectroscopic observations, respectively, we confirm the existence of inward motions in the inner penumbra and outward motions in the outer penumbra separated by a dividing line located inside the penumbra (see e.g. Zirin & Wang 1989; Wang & Zirin 1992; Molowny-Horasz

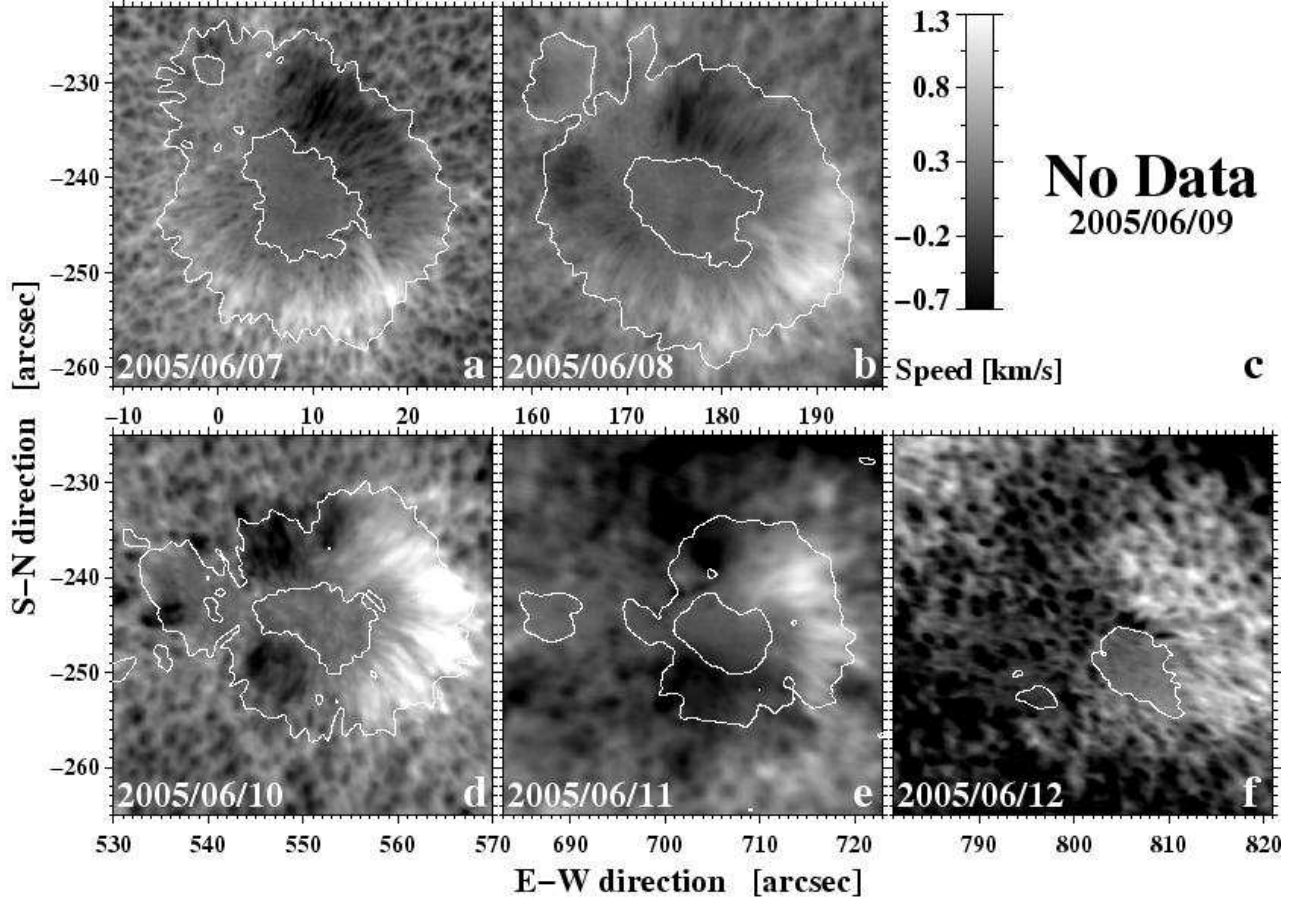


FIG. 6.— LOS dopplergram series corresponding to Figure 4 showing the Evershed flow in the sunspot. Redshifts are positive corresponding to bright areas. The gray scale in Panel c represents the magnitude of LOS velocity.

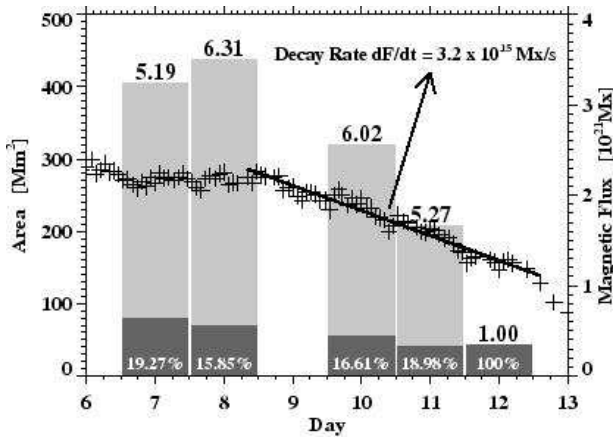


FIG. 7.— Evolution of sunspot area and magnetic flux. The light gray bars represent the penumbral area, dark gray bars correspond to the umbral area. Their sum (i.e., the whole bar) relates to the total area of the sunspot. The series of plus signs shows the evolution of the magnetic flux of the sunspot. A linear fit is applied to the decaying phase from June 9 to 12. The slope provides the overall decay rate of $3.2 \times 10^{15} \text{ Mx s}^{-1}$.

1994; Denker 1998; Sobotka et al. 1999; Bovelet & Wiehr 2003). For the first time, we demonstrate that the dividing line survives the decay process during which the sunspot lost its penumbra and fragmented. Most interestingly, we find that the moat flow in the periphery of the umbral core, i.e the residual pore, is still detectable

after the penumbra has disappeared. The outward motion, however, is not in the immediate surroundings of the pore but separated by an annular inward motion, and is much weaker than the one we find around the sunspot. We argue that the residual pore retained the flow pattern bequeathed from its parent sunspot, since sunspots and pores have historic properties, i.e., they tend to continue their past physical properties, as evidenced by the fact that large pores can be larger than small sunspots (Solanki 2003). The existence of a moat flow around umbral fragments or individual pores is still debated in the literature (e.g. Wang & Zirin 1992; Yang et al. 2003; Vargas Domínguez et al. 2007). Generally, it is believed that the large-scale organized outflow pattern of the moat around sunspots is driven by a temperature excess that builds up beneath because normal convective energy transport is inhibited. Furthermore, results from time-distance helioseismology corroborate the existence of large-scale vortex cells and downflows beneath sunspots (e.g Duvall et al. 1996; Gizon et al. 2000; Zhao et al. 2001). Already Parker (1992) suggested that individual emerging flux bundles are collared by down-draft vortex rings. Motivated by Bovelet & Wiehr (2003) who put these ideas together illustrated in a sketch (see their Figure 13) we explain our observation of a collar flow directed towards the umbra after the penumbra has disappeared as the signature of that downflow vortex cell, which is adjacent to an outer upflow and diverging vortex roll.

The inward proper motions in the inner penumbra can be very well explained in the framework of the moving-tube scenario by Schlichenmaier et al. (1998) mimicking the uncombed penumbra (Solanki & Montavon 1993). In this model the filamentary structure of the penumbra originates from the dynamics of ascending flux tubes embedded in a static background field. During the ascending phase a systematic flow develops along the flux tube, the Evershed flow. In particular penumbral grains are interpreted as the upstream footpoints of the flux tubes. As the flux tubes rise their cross-section with the $\tau = 1$ -level migrates inwards giving the visual impression that the penumbral grains move towards the umbra. Many observations have provided support for this model like most recently Rimmele & Marino (2006). The outward migration detected in the outer penumbra might be explained by the moving-tube model if the photospheric sea-serpent structure developed from the penumbral flux tubes simulated by Schlichenmaier (2002) occurs in the real Sun. We speculate that the outward flow which extends beyond the visible boundary of the sunspot penumbra is related to the propagation of ECs (see Cabrera Solana et al. 2007) but this needs still to be verified.

The observed sunspot was a peculiar follower in the sense that it was larger, more regular and more stable than its leading spot. Martínez Pillet (2002) reviewed several aspects related to the decay of leading and following sunspots and summarized the current state of knowledge of the physical mechanisms that are involved in sunspot evolution. In general, a long period of stability is rarely found in followers, they decay very fast, typically within several days or less after their formation. Following spots usually possess irregular shapes and have incomplete penumbrae. Only 3% of the observed followers develop a round shape and appear in the so-called α configuration (Bray & Loughhead 1964). It is much

more likely for the preceding sunspot to develop such a configuration which then can last from days to weeks. Hence, the observations presented in this study provide a rare exception of the aforementioned rules. We find that during the decay phase the percentage of the umbral to total sunspot area increased from 15.9% to 19.0% indicating that the penumbra decays faster than the umbra. Although the flux decay rate was almost constant ($3.2 \times 10^{15} \text{ Mx s}^{-1}$), the decay process was not uniform. We observed that the decay proceeded by the following mechanisms: fragmentation of the sunspot, flux cancellation of MMFs (of the same polarity as the sunspot) that encounter the leading opposite polarity network and plage areas, and flux transport by MMFs (of the same polarity as the sunspot) to the network and plage regions that have the same polarity of the sunspot.

In order to reconcile the discrepancies found in the large-scale flow patterns surrounding sunspots, umbral fragments, individual pores that never developed a penumbra (innate pores), and individual pores that remained from a decayed sunspot (residual pores) not only better statistics is needed. To fully understand the connection between the flow patterns and the evolution of the magnetic structures high-spatial resolution spectropolarimetric observations as provided by HINODE must complete spectroscopic and imaging observations like those presented in this investigation.

We would like to thank John Thomas, Valentina Abramenco, and Dale E. Gary for comments and discussions on the original manuscript. We also thank the referee for a number of valuable suggestions that help to improve the paper. This research has made use of NASA's Astrophysics Data System (ADS). This work was supported by NSF under grant ATM 03-42560, ATM 03-13591, ATM 02-36945, ATM 05-48952, and MRI AST 00-79482 and by NASA under grant NAG 5-13661.

REFERENCES

- Bovelet, B., & Wiehr, E. 2003, *A&A*, 412, 249
 Bray, R. J., & Loughhead, R. E. 1964, *Sunspots* (The International Astrophysics Series, London: Chapman & Hall, 1964)
 Brickhouse, N. S., & Labonte, B. J. 1988, *Sol. Phys.*, 115, 43
 Cabrera Solana, D., Bellot Rubio, L. R., Beck, C., & del Toro Iniesta, J. C. 2006, *ApJ*, 649, L41
 —. 2007, *ArXiv e-prints*, 707
 Chapman, G. A., Dobias, J. J., Preminger, D. G., & Walton, S. R. 2003, *Geophys. Res. Lett.*, 30, 27
 Choudhary, D. P., & Balasubramaniam, K. S. 2007, *ApJ*, 664, 1228
 Collados, M., Martínez, V., Ruiz, B., Deltoro, J. C., & Vazquez, M. 1994, *AA*, 0.1
 Denker, C. 1998, *Sol. Phys.*, 180, 81
 Denker, C., & Tritschler, A. 2005, *PASP*, 117, 1435
 Denker, C., Mascarinas, D., Xu, Y., Cao, W., Yang, G., Wang, H., Goode, P. R., & Rimmele, T. 2005, *Sol. Phys.*, 227, 217
 Denker, C., Deng, N., Rimmele, T. R., Tritschler, A., & Verdoni, A. 2007a, *Sol. Phys.*, 241, 411
 Denker, C., Tritschler, A., Rimmele, T. R., Richards, K., Hegwer, S. L., & Wöger, F. 2007b, *PASP*, 119, 170
 Duvall, T. L. J., D'Silva, S., Jefferies, S. M., Harvey, J. W., & Schou, J. 1996, *Nature*, 379, 235
 Evershed, J. 1909, *MNRAS*, 69, 454
 Gizon, L., Duvall, Jr., T. L., & Larsen, R. M. 2000, *Journal of Astrophysics and Astronomy*, 21, 339
 Hagenaar, H. J., & Shine, R. A. 2005, *ApJ*, 635, 659
 Harvey, K., & Harvey, J. 1973, *Sol. Phys.*, 28, 61
 Kubo, M., Shimizu, T., & Tsuneta, S. 2007, *ApJ*, 659, 812
 Leka, K. D., & Skumanich, A. 1998, *ApJ*, 507, 454
 Martínez Pillet, V. 2002, *Astronomische Nachrichten*, 323, 342
 Martínez Pillet, V., Moreno-Insertis, F., & Vazquez, M. 1993, *A&A*, 274, 521
 McIntosh, P. S. 1981, in *The Physics of Sunspots*, ed. L. E. Cram & J. H. Thomas, 7–54
 Molowny-Horas, R. 1994, *Sol. Phys.*, 154, 29
 Moreno-Insertis, F., & Vazquez, M. 1988, *A&A*, 205, 289
 November, L. J. 1986, *Appl. Opt.*, 25, 392
 November, L. J., Simon, G. W., Tarbell, T. D., & Title, A. M. 1986, in *Bulletin of the American Astronomical Society*, Vol. 18, *Bulletin of the American Astronomical Society*, 665
 November, L. J., Simon, G. W., Tarbell, T. D., Title, A. M., & Ferguson, S. H. 1987, in *Theoretical Problems in High Resolution Solar Physics*, ed. G. Athay & D. S. Spicer, 121–127
 Parker, E. N. 1992, *ApJ*, 390, 290
 Petrovay, K., Martínez Pillet, V., & van Driel-Gesztelyi, L. 1999, *Sol. Phys.*, 188, 315
 Ravindra, B. 2006, *Sol. Phys.*, 237, 297
 Rimmele, T., & Marino, J. 2006, *ApJ*, 646, 593
 Rimmele, T. R. 1994, *A&A*, 290, 972
 Rimmele, T. R., Richards, K., Hegwer, S., Fletcher, S., Gregory, S., Moretto, G., et al. 2004, *Proceedings SPIE*, 5171, 179-186
 Rouppe van der Voort, L. H. M. 2003, *A&A*, 397, 757
 Sainz Dalda, A., & Martínez Pillet, V. 2005, *ApJ*, 632, 1176
 Spirock, T. 2005, *PhD Thesis of New Jersey Institute of Technology*
 Scherrer, P. H., Bogart, R. S., Bush, R. I., Hoeksema, J. T., Kosovichev, A. G., Schou, J., et al. 1995, *Sol. Phys.*, 162, 129
 Schlichenmaier, R., Jahn, K., & Schmidt, H. U. 1998, *ApJ*, 493, L121
 Schlichenmaier, R. 2002, *Astronomische Nachrichten*, 323, 303
 Schmidt, W., Stix, M., & Wöhl, H. 1999, *A&A*, 346, 633
 Sheeley, Jr., N. R. 1969, *Sol. Phys.*, 9, 347
 Shine, R. A., Title, A. M., Tarbell, T. D., Smith, K., Frank, Z. A., & Scharmer, G. 1994, *ApJ*, 430, 413
 Sobotka, M., Brandt, P. N., & Simon, G. W. 1999, *A&A*, 348, 621
 Solanki, S. K. 2003, *Astron. Astrophys. Rev.*, 11, 153
 Solanki, S. K., & Montavon, C. A. P. 1993, *A&A*, 275, 283

- Vargas Domínguez, S., Bonet, J. A., Martínez Pillet, V., Katsukawa, Y., Kitakoshi, Y., & Rouppe van der Voort, L. 2007, ApJ, 660, L165
- Wang, H., & Zirin, H. 1992, Sol. Phys., 140, 41
- Wang, H., Denker, C., Spirock, T., Goode, P. R., Yang, S., Marquette, W., Varsik, J., Fear, R. J., Nenow, J. & Dingley, D. D. 1998, Sol. Phys., 183, 1
- Yang, G., Xu, Y., Wang, H., & Denker, C. 2003, ApJ, 597, 1190
- Yurchyshyn, V. B., & Wang, H. 2001, Sol. Phys., 203, 233
- Zhao, J., Kosovichev, A. G., & Duvall, Jr., T. L. 2001, ApJ, 557, 384
- Zirin, H., & Wang, H. 1989, Sol. Phys., 119, 245
- Zwaan, C. 1992, in NATO ASIC Proc. 375: Sunspots. Theory and Observations, ed. J. H. Thomas & N. O. Weiss, 75–100